STRUCTURAL BIOLOGY COMMUNICATIONS

ISSN 2053-230X

Crystal structures of *Leishmania mexicana* arginase complexed with α,α-disubstituted boronic amino-acid inhibitors

Yang Hai[a] and David W. Christianson[a,b]*

[a]Roy and Diana Vagelos Laboratories, Department of Chemistry, University of Pennsylvania, Philadelphia, PA 19104, USA, and [b]Radcliffe Institute for Advanced Study and Department of Chemistry and Chemical Biology, Harvard University, Cambridge, MA 02138, USA. *Correspondence e-mail: chris@sas.upenn.edu

Received 14 January 2016
Accepted 1 March 2016

Edited by R. A. Pauptit, Macclesfield, England

Keywords: *Leishmania mexicana*; arginase; α,α-disubstituted boronic amino-acid inhibitors.

PDB references: *L. mexicana* arginase, complex with ABH_{PE}, 5hj9; complex with ABH_{DP}, 5hja

Supporting information: this article has supporting information at journals.iucr.org/f

Leishmania arginase is a potential drug target for the treatment of leishmaniasis because this binuclear manganese metalloenzyme initiates *de novo* polyamine biosynthesis by catalyzing the hydrolysis of L-arginine to generate L-ornithine and urea. The product L-ornithine subsequently undergoes decarboxylation to yield putrescine, which in turn is utilized for spermidine biosynthesis. Polyamines such as spermidine are essential for the growth and survival of the parasite, so inhibition of enzymes in the polyamine-biosynthetic pathway comprises an effective strategy for treating parasitic infections. To this end, two X-ray crystal structures of *L. mexicana* arginase complexed with α,α-disubstituted boronic amino-acid inhibitors based on the molecular scaffold of 2-(*S*)-amino-6-boronohexanoic acid are now reported. Structural comparisons with human and parasitic arginase complexes reveal interesting differences in the binding modes of the additional α-substituents, *i.e.* the D side chains, of these inhibitors. Subtle differences in the three-dimensional contours of the outer active-site rims among arginases from different species lead to different conformations of the D side chains and thus different inhibitor-affinity trends. The structures suggest that it is possible to maintain affinity while fine-tuning intermolecular interactions of the D side chain of α,α-disubstituted boronic amino-acid inhibitors in the search for isozyme-specific and species-specific arginase inhibitors.

1. Introduction

Leishmaniasis is a neglected tropical disease caused by more than 20 different *Leishmania* species prevalent in nearly 100 countries, with 1.3 million new cases diagnosed annually (Crompton, 2013). There are three main forms of the disease: visceral leishmaniasis, which affects the spleen, liver and bone marrow, and is usually fatal if left untreated; cutaneous leishmaniasis, which is characterized by large, disfiguring skin lesions; and mucocutaneous leishmaniasis, which causes painful lesions in nasal and oropharyngeal tissues. It is estimated that 20 000–40 000 people die from visceral leishmaniasis annually (Alvar *et al.*, 2012). The occurrence of leishmaniasis is on the rise in Western countries owing to travel to and from endemic regions by military and civilian personnel (Antinori *et al.*, 2005), so this neglected tropical disease comprises an increasingly prominent threat to public health.

Treatment options for patients diagnosed with leishmaniasis vary depending upon the parasite species involved, the organs and tissues affected, and the quality of healthcare available (Desjeux, 1996, 2001). For example, many cases of cutaneous leishmaniasis can resolve spontaneously, and those that do not generally respond to treatment with pentavalent antimony-

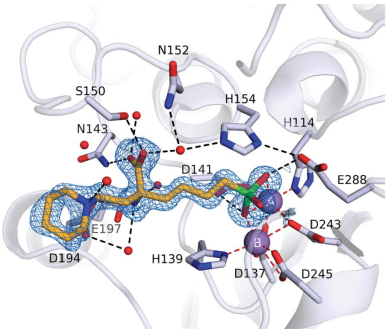

based drugs. Other drugs currently in use for the treatment of cutaneous or visceral leishmaniasis include amphotericin B, pentamidine and miltefosine. Unfortunately, no single leishmaniasis treatment option is ideal owing to financial expense (especially for patients in developing countries), long drug-treatment regimens and side effects. Moreover, the emergence of resistance to currently existing drugs suggests that there is an urgent need for new pharmacological targets for leishmaniasis therapy (Sundar, 2001; Pérez-Victoria *et al.*, 2002).

L. mexicana arginase (LmARG) is considered to be an attractive drug target in the exploration of new therapeutic approaches. This binuclear manganese metalloenzyme initiates the first step of *de novo* polyamine biosynthesis by catalyzing the hydrolysis of L-arginine to generate L-ornithine and urea (Ash *et al.*, 2000; Christianson, 2005; Fig. 1*a*); L-ornithine subsequently undergoes decarboxylation to yield putrescine, a polyamine building block (Heby *et al.*, 2003, 2007). Studies of arginase-knockout mutants in *Leishmania* parasites confirm that arginase activity is essential for parasite viability and infectivity (Roberts *et al.*, 2004; Reguera *et al.*, 2009; da Silva, Maquiaveli *et al.*, 2012; da Silva, Zampieri *et al.*, 2012). Crystal structures of LmARG complexed with first-generation L-amino-acid inhibitors such as 2-(*S*)-amino-6-boronohexanoic acid (ABH; Fig. 1*b*) revealed the molecular basis of affinity and inhibitory activity (D'Antonio *et al.*, 2013), thereby setting the stage for the design and evaluation of second-generation inhibitors.

To expand the chemical space of arginase-inhibitor design, novel α,α-disubstituted boronic acid inhibitors based on ABH have been developed and evaluated against human arginase I, human arginase II, *Plasmodium falciparum* arginase and *Schistosoma mansoni* arginase (Ilies *et al.*, 2011; Golebiowski *et al.*, 2013; Van Zandt *et al.*, 2013; Hai *et al.*, 2014). While the L-boronic acid side chain of these inhibitors binds in the active-site cleft in an identical fashion to that of the parent compound ABH, the additional D side chain of these inhibitors can make new interactions in the outer rim of the active site.

Here, we report the crystal structures of LmARG with the α,α-disubstituted boronic acid inhibitors (*R*)-2-amino-6-borono-2-[2-(piperidin-1-yl)ethyl]hexanoic acid (ABH_{PE}) and (*R*)-2-amino-6-borono-2-[1-(3,4-dichlorobenzyl)piperidin-4-yl]-hexanoic acid (ABH_{DP}) (Fig. 1*c*; Golebiowski *et al.*, 2013; Van Zandt *et al.*, 2013). Structural comparisons with human and parasitic arginase complexes reveal interesting differences in the binding modes of the D side chains of these inhibitors. Even though the active-site clefts of these enzymes are highly conserved, the outer rims are not. Accordingly, different conformations are observed for the D side chains. As a proof of concept, our structures suggest that it is possible to maintain affinity while fine-tuning the intermolecular interactions of the D side chain of α,α-disubstituted boronic amino-acid inhibitors in the search for isozyme-specific and species-specific arginase inhibitors.

2. Materials and methods

2.1. Crystallization

Recombinant LmARG was expressed and purified as reported previously (D'Antonio *et al.*, 2013). The LmARG–ABH_{PE} complex was crystallized using the sitting-drop vapor-diffusion method at 21°C by mixing 1 µl LmARG solution (6 mg ml^{-1} protein pre-incubated with 10 m*M* ABH_{PE} in 50 m*M* Bicine pH 8.5, 100 µ*M* $MnCl_2$, 1 m*M* TCEP, 5% glycerol, 2.5% DMSO) with 1 µl precipitant solution (0.1 *M*

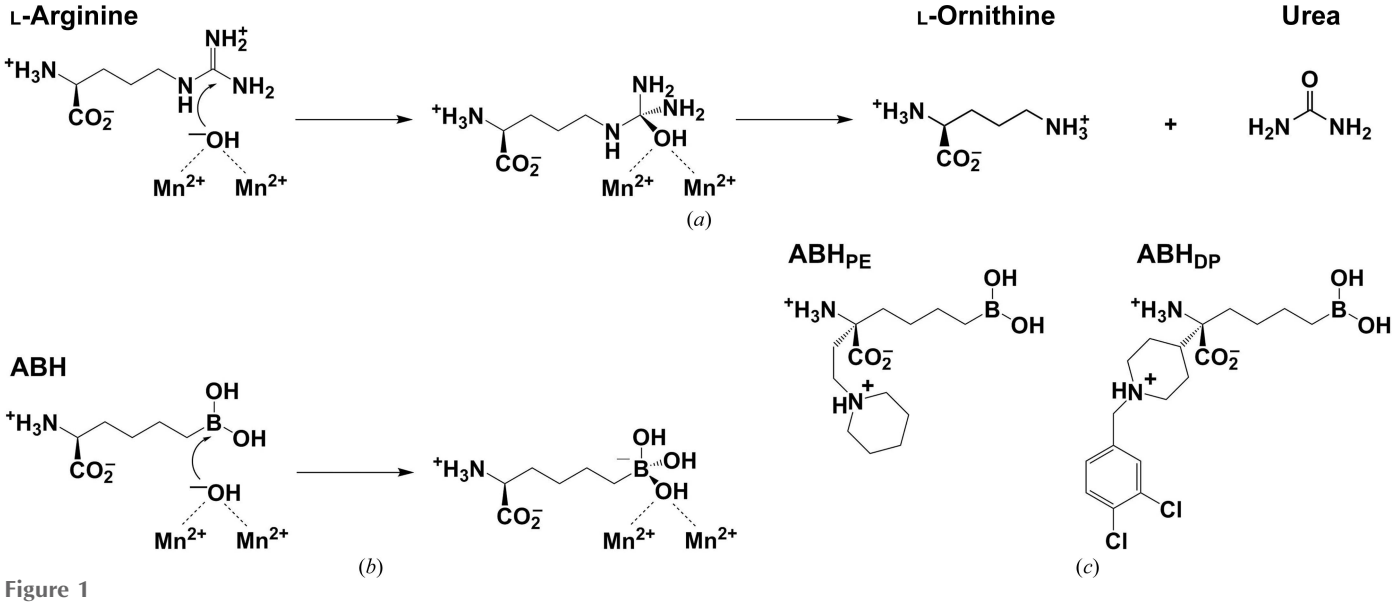

Figure 1
(*a*) Arginase utilizes a metal-bridging hydroxide ion to catalyze the hydrolysis of L-arginine to form L-ornithine and urea. (*b*) The boronic acid analogue of L-arginine, 2-(*S*)-amino-6-boronohexanoic acid (ABH), undergoes nucleophilic attack by the metal-bridging hydroxide ion to yield a tetrahedral boronate anion that mimics the tetrahedral intermediate and its flanking transition states in the arginase reaction. (*c*) The arginase inhibitors (*R*)-2-amino-6-borono-2-[2-(piperidin-1-yl)ethyl]hexanoic acid (ABH_{PE}) and (*R*)-2-amino-6-borono-2-[1-(3,4-dichlorobenzyl)piperidin-4-yl]hexanoic acid (ABH_{DP}).

Table 1
Data-collection and refinement statistics.

Values in parentheses are for the highest resolution shell.

	LmARG–ABH_{PE}	LmARG–ABH_{DP}
PDB entry	5hj9	5hja
Data collection		
Beamline	X29, NSLS	X29, NSLS
Wavelength (Å)	1.075	1.075
Temperature (K)	100	100
Detector	ADSC Q315	ADSC Q315
Space group	*R*3:*H*	*R*3:*H*
Resolution (Å)	50.0–1.28	50.0–1.65
Total reflections measured	1041671	281614
Unique reflections measured	86060	40479
Unit-cell parameters (Å)	$a = b = 89.1$, $c = 113.6$	$a = b = 88.9$, $c = 113.9$
Completeness (%)	99.4 (94.6)	99.5 (95.3)
$\langle I/\sigma(I)\rangle$	29.3 (1.2)	22.4 (2.1)
R_{sym}†	0.091 (1.202)	0.089 (0.730)
$R_{p.i.m.}$‡	0.029 (0.509)	0.035 (0.316)
Multiplicity	12.1 (8.5)	7.0 (5.7)
$CC_{1/2}$§	0.956 (0.510)	0.987 (0.817)
Overall *B* factor from Wilson plot (Å^2)	16	24
Twin fraction	0.15	0.08
Refinement		
No. of reflections		
Refinement	77901	36600
Test set	8159	3879
Twin law	$h, -h-k, -l$	$h, -h-k, -l$
R_{work}¶ (%)	14.6 (30.1)	18.7 (31.8)
R_{free}¶ (%)	15.9 (31.0)	21.2 (34.5)
No. of non-H atoms per monomer		
Protein	2425	2326
Solvent	200	146
Ligands	67	36
Mn^{2+} ions	2	2
R.m.s. deviations		
Bonds (Å)	0.012	0.004
Angles (°)	1.3	0.8
Average *B* factors (Å^2)		
Protein	25	35
Solvent	35	40
Mn^{2+} ions	14	25
Inhibitor	30	55
Other ligands	32	28
Ramachandran		
Favored†† (%)	97.3	96.6
Outliers†† (%)	0.6	0.33

† $R_{merge} = \sum_{hkl}\sum_i |I_i(hkl) - \langle I(hkl)\rangle| / \sum_{hkl}\sum_i I_i(hkl)$, where $I(hkl)$ is the intensity of reflection hkl, $\sum_{hkl}$ is the sum over all reflections and $\sum_i$ is the sum over i measurements of reflection hkl. ‡ $R_{p.i.m.} = \sum_{hkl}\{1/[N(hkl)-1]\}^{1/2}\sum_i |I_i(hkl) - \langle I(hkl)\rangle| / \sum_{hkl}\sum_i I_i(hkl)$, where $N(hkl)$ is the number of observations (multiplicity) and $\langle I(hkl)\rangle$ is the average intensity calculated from replicate data. § $CC_{1/2} = \sigma_\tau^2/(\sigma_\tau^2 + \sigma_\varepsilon^2)$, where σ_τ^2 is the true measurement-error variance and σ_ε^2 is the independent measurement-error variance. ¶ $R_{work} = \sum_{hkl} ||F_{obs}| - |F_{calc}|| / \sum_{hkl} |F_{obs}|$ for reflections contained in the working set. $R_{free} = \sum_{hkl} ||F_{obs}| - |F_{calc}|| / \sum_{hkl} |F_{obs}|$ for reflections contained in the test set held aside during refinement. $|F_{obs}|$ and $|F_{calc}|$ are the observed and calculated structure-factor amplitudes, respectively. †† Calculated with *MolProbity*.

HEPES pH 7.5, 25% PEG 3350). The LmARG–ABH_{DP} complex was crystallized in a similar fashion by mixing 1 µl LmARG solution (6 mg ml^{-1} protein pre-incubated with 10 m*M* ABH_{DP} in 50 m*M* Bicine pH 8.5, 100 µ*M* $MnCl_2$, 1 m*M* TCEP, 5% glycerol, 2.5% DMSO) with 1 µl precipitant solution (0.1 *M* HEPES pH 7.2, 22% PEG 3350) at 21°C. Crystals appeared in 3 d and were soaked in a cryoprotectant solution comprised of precipitant solution supplemented with 25–30% glycerol prior to flash-cooling in liquid nitrogen.

Table 2
Inhibitory activity of ABH derivatives.

Inhibitor	IC_{50} (µ*M*)	K_i (µ*M*)
ABH, *S*-isomer (L)	1.3 ± 0.2	0.9 ± 0.1
ABH_{PE}, *S*-isomer (L)	2.1 ± 0.3	1.4 ± 0.2
ABH_{DP}, racemic (DL)	1.7 ± 0.4	1.1 ± 0.3

2.2. X-ray data collection and processing

X-ray diffraction data were collected on beamline X29 at the National Synchrotron Light Source (NSLS), Brookhaven National Laboratory, New York, USA. Diffraction data were integrated and scaled with *HKL*-2000 (Otwinowski & Minor, 1997). Data-collection and reduction statistics are listed in Table 1. The structure was determined by molecular replacement using *Phaser* (McCoy *et al.*, 2007) as implemented in the *CCP*4 suite of programs, with the atomic coordinates of unliganded LmARG (PDB entry 4ity; D'Antonio *et al.*, 2013) utilized as a search probe for rotation-function and translation-function calculations. Iterative cycles of refinement and model building were performed using *PHENIX* (Adams *et al.*, 2010) and *Coot* (Emsley *et al.*, 2010), respectively. The hemihedral twinning operator $h, -h-k, -l$ was included in the refinement strategy as described previously (D'Antonio *et al.*, 2013). Solvent molecules and inhibitors were added in the final stages of refinement for each structure. The quality of each final model was verified with *MolProbity* (Chen *et al.*, 2010). The refinement statistics are reported in Table 1. Protein structure figures were prepared with *PyMOL* (http://www.pymol.org) and *Adobe Photoshop CS*.

2.3. Inhibitory activity assays

Arginase activity was measured using a colorimetric assay with slight modifications (Archibald, 1945). Briefly, 0.5–150 m*M* L-arginine pH 8.0 was added to a solution consisting of 50 m*M* 4-(2-hydroxyethyl)piperazine-1-propanesulfonic acid (EPPS) pH 8.0, 100 µ*M* $MnCl_2$ and the reaction was initiated by adding 1 µ*M* LmARG in a total volume of 170 µl at 21°C. The reaction was terminated after 20 min using 30 µl of a 3:1(*v*:*v*) concentrated acid/dye solution [1:3:1(*v*:*v*:*v*) H_2SO_4:H_3PO_4:H_2O and 245 m*M* α-isonitrosopropiophenone in ethanol]. Samples were heated to 90°C for 1 h in a thermocycler to ensure complete reaction of urea with the dye. To quantify urea formation, the absorbance of each sample was measured at λ = 550 nm using a Tecan Infinite M1000 Pro Microplate Reader. Kinetic parameters were determined using *GraphPad Prism*. For IC_{50} determinations, 30 m*M* L-arginine was used and the K_i values for ABH_{PE} and ABH_{DP} were calculated based on the Cheng–Prusoff equation [$K_i = IC_{50}/(1 + [S]/K_m)$] (Cheng & Prusoff, 1973).

3. Results and discussion

In comparison with the parent inhibitor ABH, the α,α-disubstituted boronic amino acids ABH_{PE} and ABH_{DP} exhibit modestly improved affinity for *S. mansoni* arginase (5.0-fold and 2.4-fold, respectively; Hai *et al.*, 2014), modestly improved

inhibitory potency (IC_{50}) against human arginase I (6.5-fold and 7.4-fold, respectively; Van Zandt *et al.*, 2013) and modestly improved inhibitory potency against human arginase II (3.8-fold and 7.4-fold, respectively; Golebiowski *et al.*, 2013). However, neither ABH_{PE} nor ABH_{DP} exhibit improved inhibitory potency against LmARG (Table 2, Fig. 2). Even so, since the ABH_{DP} sample is a racemic mixture, the effective IC_{50} of the L-boronic acid side-chain enantiomer should be twofold lower than that measured for the racemic mixture, since only the L-boronic acid side-chain enantiomer binds to the enzyme (see below).

The overall structures of LmARG complexed with ABH_{PE} and ABH_{DP} (Fig. 3) are essentially identical to the structure of the LmARG–ABH complex (PDB entry 4iu0; D'Antonio *et al.*, 2013), with r.m.s. deviations of 0.26 Å (ABH_{PE}) and 0.17 Å (ABH_{DP}) for 289 and 286 C^{α} atoms, respectively. Although racemic ABH_{DP} was used in the crystallization experiment, the electron-density map unambiguously shows that the L stereoisomer binds exclusively in the active site, as also observed for binding to *S. mansoni* arginase (Hai *et al.*, 2014). The boronic acid moiety of each inhibitor undergoes nucleophilic attack by the metal-bridging hydroxide ion to form a tetrahedral boronate anion, as observed for the parent compound ABH (Fig. 1*b*; D'Antonio *et al.*, 2013), a well studied competitive inhibitor (Riley *et al.*, 2011). This tetrahedral species mimics the tetrahedral intermediate and its flanking transition states in the arginase reaction (Fig. 1*a*). Metal-coordination and hydrogen-bond interactions of the tetrahedral boronate anions in the LmARG complexes with ABH, ABH_{PE} and ABH_{DP} are compared in Table 3.

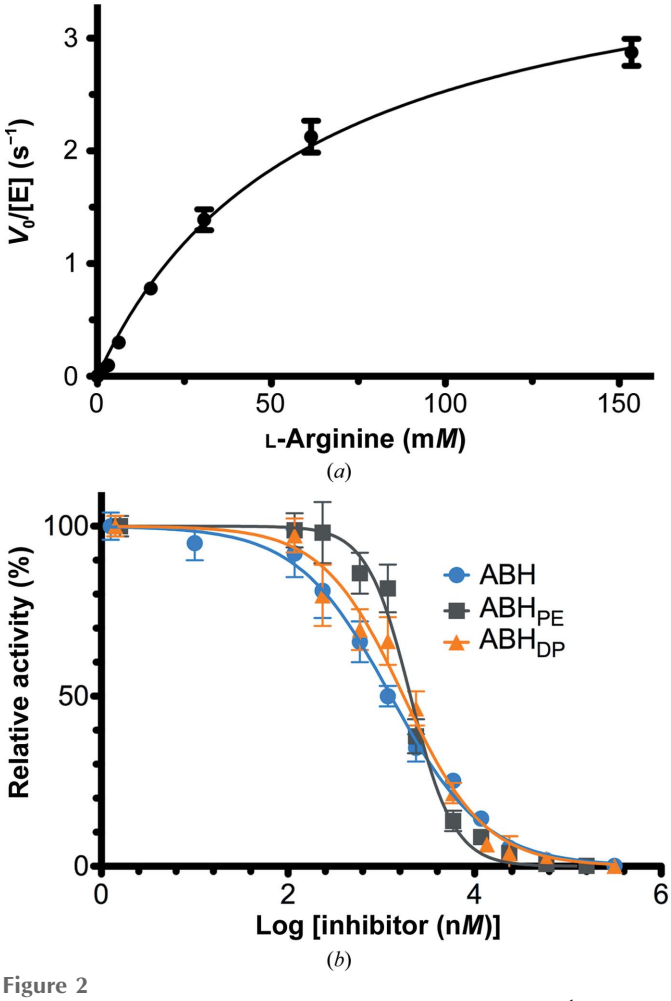

Figure 2
(*a*) Steady-state kinetics of LmARG yield k_{cat} = 4.1 ± 0.2 s^{-1} and K_m = 61 ± 6 m*M*. (*b*) Inhibitory activity assays of LmARG; IC_{50} values are recorded in Table 2.

Table 3
Intermolecular interactions of the boronate anion.

Interaction	Distance (Å) ABH	ABH_{PE}	ABH_{DP}
O1···Mn_A^{2+}	2.2	2.2	1.9
O1···Mn_B^{2+}	2.2	2.0	2.2
O1···Asp141	2.6	2.7	2.7
O2···Mn_A^{2+}	2.3	2.2	2.2
O3···Thr257	2.9	2.7	2.6

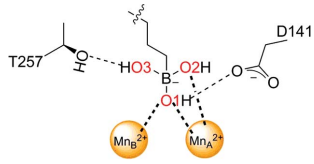

The α-carboxylate and α-amino groups are recognized by the conserved L-amino-acid recognition motifs, which saturate the hydrogen-bonding potential and ensure strict molecular recognition of the proper amino-acid stereoisomer. The α-carboxylate group of ABH_{PE} accepts hydrogen bonds from Asn143, Ser150 and two water molecules, and the α-amino group donates hydrogen bonds to Asp194 and two water molecules. It is interesting that the stereoselectivity for L-amino-acid binding is maintained by four water-mediated and three direct hydrogen bonds to the protein. In the LmARG–ABH_{DP} complex, however, the D side chain blocks a water molecule mediating the hydrogen bond between Asp194 and the α-amino group (the direct hydrogen bond between Asp194 and the α-amino group is maintained). Nevertheless, a superposition of the LmARG complexes with ABH, ABH_{PE} and ABH_{DP} shows that the binding modes of the parent ABH backbones are essentially identical (Fig. 4).

Despite similar binding modes for the L-amino-acid portion of each inhibitor, the additional D side chains adopt different conformations (Fig. 4). In the LmARG–ABH_{PE} complex the piperidine ring is unambiguously assigned as a chair conformation based on high-resolution electron density (Fig. 3*a*). Remarkably, the D side chain of ABH_{PE} makes no direct interaction with LmARG; the protonated tertiary amino group of the piperidine ring is oriented away from Asp194 and forms a hydrogen bond to a water molecule. The binding mode of ABH_{PE} with LmARG contrasts with that observed in *S. mansoni* arginase (SmARG), where the piperidine amino group donates a hydrogen bond to Asp213 (which corresponds to Asp194 in LmARG; Hai *et al.*, 2014). The binding mode of ABH_{PE} in SmARG is unique, since only this particular enzyme has a groove that accommodates the piperidine ring of ABH_{PE} (Fig. 5). Notably, the piperidine ring of ABH_{PE} does not interact directly with the active-site residues in human arginases I and II, although a water-mediated interaction is observed in the human arginase I–ABH_{PE} complex (Van Zandt *et al.*, 2013).

In the LmARG–ABH_{DP} complex, the D side chain of LmARG–ABH_{DP} is characterized by weak and broken electron density, suggesting that it is largely disordered. Regardless, the piperidine ring is best modeled in a chair conformation with the protonated tertiary amino group donating a hydrogen bond to Asp194 (Fig. 3*b*). Interestingly, the dichlorobenzyl group packs against the Ala192 region. This conformation is unique to LmARG, since Ala192 is replaced by a conserved aspartate in human arginase I, human arginase II and SmARG. The bulky, charged aspartate at this position in SmARG causes the D side chain of ABH_{DP} to adopt an alternative conformation (Fig. 5*f*).

It is somewhat surprising that the additional D side-chain substituents of ABH_{PE} and ABH_{DP} do not confer some degree of affinity enhancement relative to ABH. Even though the additional side chains do not make any polar interactions with protein residues, these side chains bind in the so-called 'D-cleft' (Ilies *et al.*, 2011), making van der Waals contacts and displacing the associated water molecules to the bulk solvent. Presumably, the entropic gain provided by the release of water to bulk solvent upon enzyme–inhibitor complexation is offset by the conformational entropic cost of side-chain binding in the D-cleft. Even so, these structures will inform the future design of alternative D substituents for an α,α-disubstituted

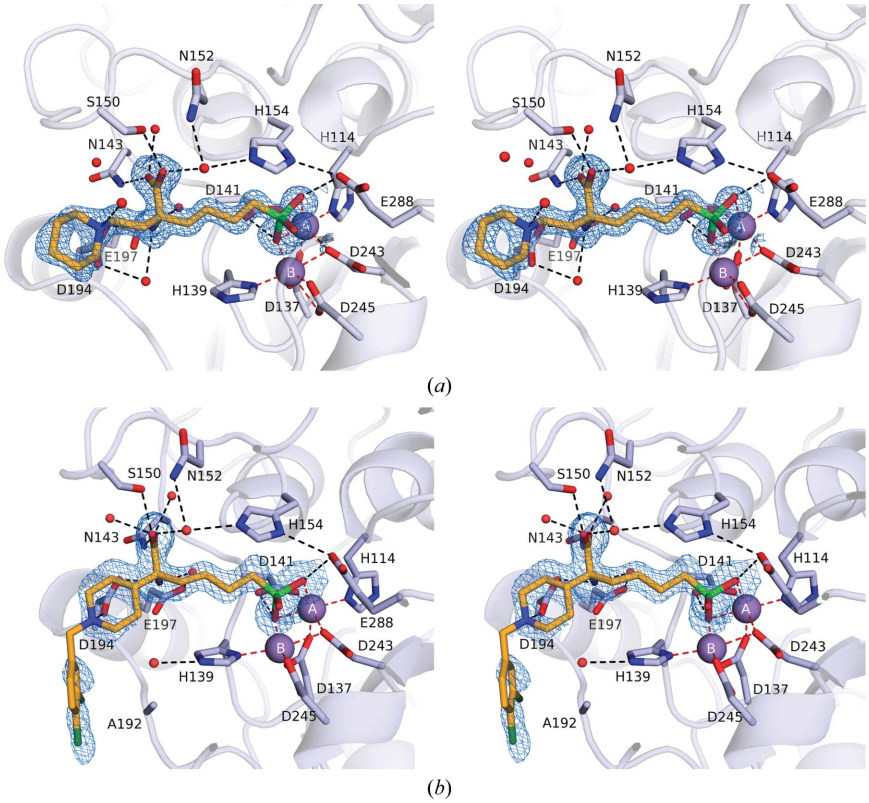

Figure 3
(*a*) Simulated-annealing OMIT map of ABH_{PE} bound to LmARG contoured at 2.5σ. Mn^{2+} ions are shown as purple spheres. Ligand atoms are color-coded as follows: C, orange; N, blue; O, red; Cl, dark green; B, green. Metal-coordination and hydrogen-bond interactions are shown as red and black dashed lines, respectively. (*b*) Simulated-annealing OMIT map of ABH_{DP} bound to LmARG contoured at 2.5σ and color-coded as in (*a*).

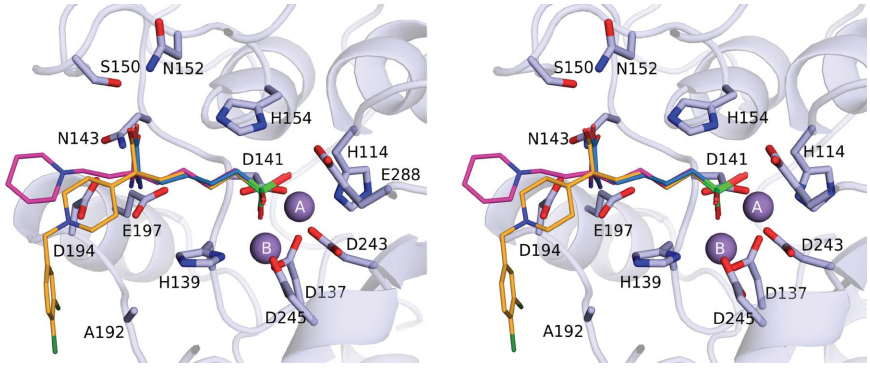

Figure 4
Superposition of the LmARG–ABH complex (blue C atoms), the LmARG–ABH_{PE} complex (magenta C atoms) and the LmARG–ABH_{DP} complex (orange C atoms) reveals similar overall binding modes of the ABH-based scaffold of each inhibitor but different binding conformations for the D side chains of ABH_{PE} and ABH_{DP}

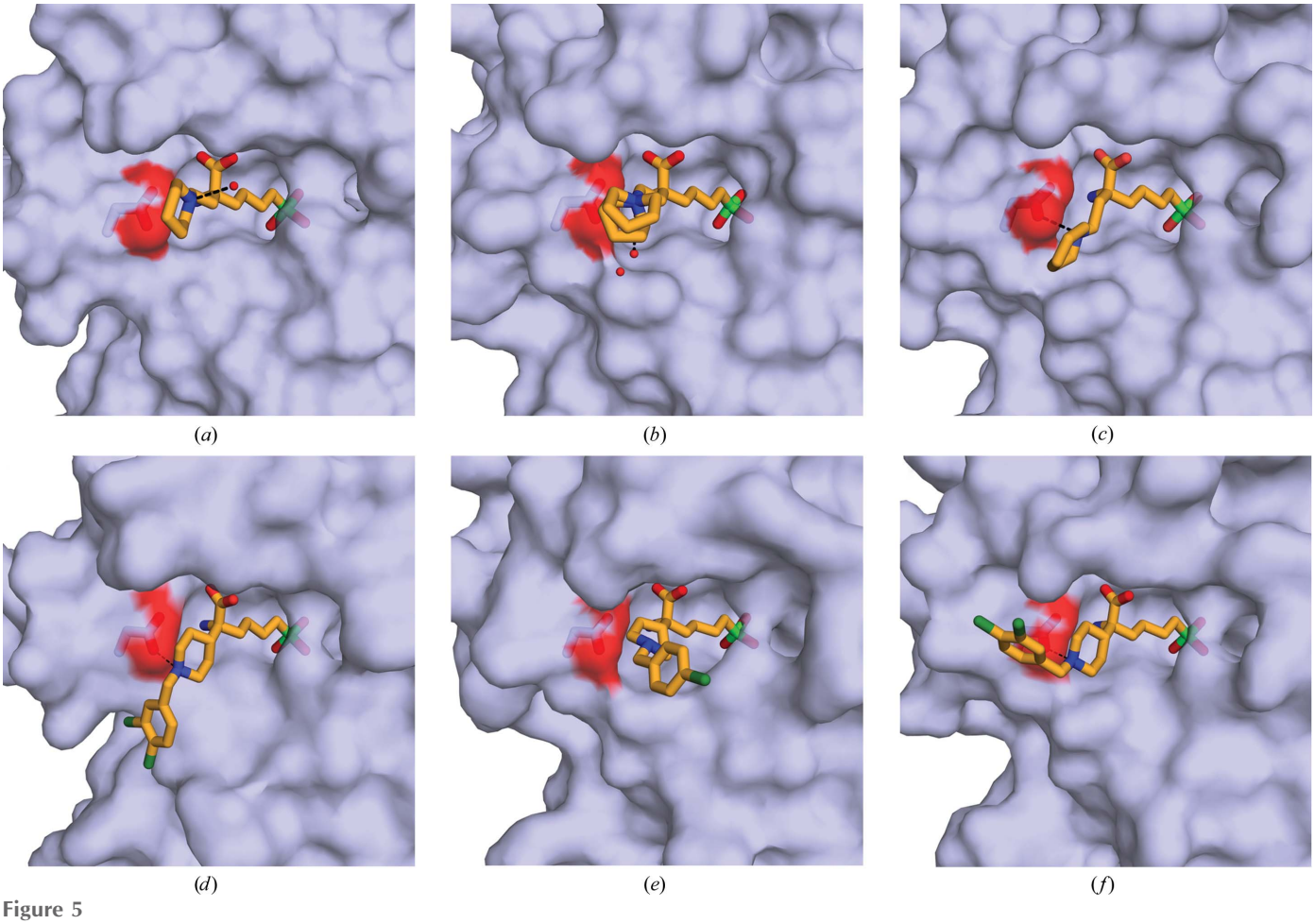

Figure 5
Comparison of α,α-disubstituted boronic acid inhibitors bound to arginases from different species. (*a*) LmARG–ABH_{PE} complex. (*b*) Human arginase I–ABH_{PE} complex (PDB entry 4hww; Van Zandt *et al.*, 2013). (*c*) SmARG–ABH_{PE} complex (PDB entry 4q3s; Hai *et al.*, 2014). (*d*) LmARG–ABH_{DP} complex. (*e*) Human arginase II–ABH_{CP} complex (PDB entry 4ixv; Golebiowski *et al.*, 2013). (*f*) SmARG–ABH_{DP} complex (PDB entry 4q3r; Hai *et al.*, 2014). The conserved aspartate residues (Asp194 in LmARG) potentially interacting with the piperidine group of the D side chain are highlighted as sticks. Ligand atoms are color-coded as follows: C, bright orange; N, blue; O, red; Cl, dark green; B, green. Hydrogen bonds are shown as black dashed lines.

ABH inhibitor. For example, a bulkier side-chain substituent might thwart the molecular disorder observed for the D side chain of ABH_{DP}. The three-dimensional contour and chemical nature of the D-cleft region can vary in arginases from different species and it is conceivable that interactions of inhibitor substituents in this region could contribute to isozyme or species selectivity.

4. Conclusions

In conclusion, the crystal structures of LmARG in complex with α,α-disubstituted boronic amino-acid inhibitors reported here provide important clues regarding the design of next-generation inhibitors based on the ABH scaffold. While the inhibitory potency of ABH against LmARG is not enhanced by the additional D side-chain substituents present in ABH_{PE} and ABH_{DP}, the inhibitory potency is not compromised either. Thus, ABH_{PE} and ABH_{DP} comprise useful starting points for the design of modified D side-chain substituents that may confer improvements in inhibitory potency and/or species selectivity for arginase inhibition. Future studies in this regard will be reported in due course.

Acknowledgements

We thank Dr Michael C. Van Zandt of New England Discovery Partners for the generous gift of samples of ABH_{PE} and ABH_{DP}, and we are grateful to Drs Edward D'Antonio and Buddy Ullman for helpful scientific discussions. We thank the National Synchrotron Light Source at Brookhaven National Laboratory (beamline X29) for access to X-ray crystallographic data-collection facilities. Finally, we thank the NIH for grant GM49758 in support of this research.

References

Adams, P. D. *et al.* (2010). *Acta Cryst.* D**66**, 213–221.
Alvar, J., Vélez, I. D., Bern, C., Herrero, M., Desjeux, P., Cano, J., Jannin, J. & den Boer, M. (2012). *PLoS One*, **7**, e35671.
Antinori, S., Gianelli, E., Calattini, S., Longhi, E., Gramiccia, M. & Corbellino, M. (2005). *Clin. Microbiol. Infect.* **11**, 343–346.
Archibald, R. M. (1945). *J. Biol. Chem.* **157**, 507–518.

Ash, D. E., Cox, J. D. & Christianson, D. W. (2000). *Met. Ions Biol. Syst.* **37**, 407–428.
Chen, V. B., Arendall, W. B., Headd, J. J., Keedy, D. A., Immormino, R. M., Kapral, G. J., Murray, L. W., Richardson, J. S. & Richardson, D. C. (2010). *Acta Cryst.* D**66**, 12–21.
Cheng, Y. & Prusoff, W. H. (1973). *Biochem. Pharmacol.* **22**, 3099–3108.
Christianson, D. W. (2005). *Acc. Chem. Res.* **38**, 191–201.
Crompton, D. W. T. (2013). Editor. *Sustaining the Drive to Overcome the Global Impact of Neglected Tropical Diseases: Second WHO Report on Neglected Diseases*. Geneva: World Health Organization.
D'Antonio, E. L., Ullman, B., Roberts, S. C., Dixit, U. G., Wilson, M. E., Hai, Y. & Christianson, D. W. (2013). *Arch. Biochem. Biophys.* **535**, 163–176.
Desjeux, P. (1996). *Clin. Dermatol.* **14**, 417–423.
Desjeux, P. (2001). *Trans. R. Soc. Trop. Med. Hyg.* **95**, 239–243.
Emsley, P., Lohkamp, B., Scott, W. G. & Cowtan, K. (2010). *Acta Cryst.* D**66**, 486–501.
Golebiowski, A. *et al.* (2013). *Bioorg. Med. Chem. Lett.* **23**, 4837–4841.
Hai, Y., Edwards, J. E., Van Zandt, M. C., Hoffmann, K. F. & Christianson, D. W. (2014). *Biochemistry*, **53**, 4671–4684.
Heby, O., Persson, L. & Rentala, M. (2007). *Amino Acids*, **33**, 359–366.
Heby, O., Roberts, S. C. & Ullman, B. (2003). *Biochem. Soc. Trans.* **31**, 415–419.
Ilies, M., Di Costanzo, L., Dowling, D. P., Thorn, K. J. & Christianson, D. W. (2011). *J. Med. Chem.* **54**, 5432–5443.
McCoy, A. J., Grosse-Kunstleve, R. W., Adams, P. D., Winn, M. D., Storoni, L. C. & Read, R. J. (2007). *J. Appl. Cryst.* **40**, 658–674.
Otwinowski, Z. & Minor, W. (1997). *Methods Enzymol.* **276**, 307–326.
Pérez-Victoria, J. M., Di Pietro, A., Barron, D., Ravelo, A. G., Castanys, S. & Gamarro, F. (2002). *Curr. Drug Targets*, **3**, 311–333.
Reguera, R. M., Balaña-Fouce, R., Showalter, M., Hickerson, S. & Beverley, S. M. (2009). *Mol. Biochem. Parasitol.* **165**, 48–56.
Riley, E., Roberts, S. C. & Ullman, B. (2011). *Int. J. Parasitol.* **41**, 545–552.
Roberts, S. C., Tancer, M. J., Polinsky, M. R., Gibson, K. M., Heby, O. & Ullman, B. (2004). *J. Biol. Chem.* **279**, 23668–23678.
Silva, E. R. da, Maquiaveli, C. C. & Magalhães, P. P. (2012). *Exp. Parasitol.* **130**, 183–188.
Silva, M. F. da, Zampieri, R. A., Muxel, S. M., Beverley, S. M. & Floeter-Winter, L. M. (2012). *PLoS One*, **7**, e34022.
Sundar, S. (2001). *Trop. Med. Int. Health*, **6**, 849–854.
Van Zandt, M. C. *et al.* (2013). *J. Med. Chem.* **56**, 2568–2580.